Contemporary Mathematics
https://ojs.wiserpub.com/index.php/CM/

Research Article

Green Energy Generation Dynamical System: Fractal-Fractional Mathematical Modeling with AI-Driven Data Analysis

Hasib Khan[1*], Hadeel Bin Amer[2], Wafa F. Alfwzan[3], Jehad Alzabut[1], Rajermani Thinakaran[4]

[1] Department of Mathematics and Sciences, Prince Sultan University, Riyadh 11586, Saudi Arabia
[2] Department of Computer Science, College of Computer and Information Sciences, Majmaah University, Al-Majmaah 11952, Saudi Arabia
[3] Department of Mathematical Sciences, College of Science, Princess Nourah bint Abdulrahman University, Riyadh 11671, Saudi Arabia
[4] Faculty of Data Science and Information Technology, INTI International University, Nilai 71800, Malaysia
E-mail: hkhan@psu.edu.sa

Received: 9 December 2025; **Revised:** 20 January 2026; **Accepted:** 6 February 2026

Abstract: As the demand for renewable energy increases, it becomes more vital to efficiently integrate different resources such as wind and solar energy. This study illustrates a novel integrated mechanism for analyzing a green energy generation dynamical system utilizing the Fractal-Fractional (FF) sense of operators. We give a robust deep learning framework designed to successfully model the complex interactions and nonlinear characteristics of these energy sources. This mechanism leverages FF-calculus to improve the model's efficiency, incorporating comprehensive error analysis and advanced pattern recognition techniques. Our mathematical analysis confirms the feasibility of both the initial and parametric values of the model, demonstrating its robustness. The existence criteria, uniqueness results, and stability were also confirmed in the theoretical aspect of the work. Computational results show that the proposed hybrid system of energy significantly outperforms traditional solar-only systems, achieving an efficiency improvement of approximately 25% in energy generation. This work not only supports the existing knowledge in renewable energy but also provides a practical approach for optimizing green power generation systems by the use of artificial intelligence as a process innovation.

***Keywords*:** green energy, wind-power hybrid model, mathematical analysis, computational results, regression analysis, pattern recognition

MSC: 92B05, 93B24, 34K60, 34M04

Abbreviation

EMS	Electromagnetic System
FDEs	Fractional Differential Equations
LC	Lipchitz Condition
HUS	Hyers-Ulam Stability

Copyright ©2026 Hasib Khan, et al.
DOI: https://doi.org/10.37256/cm.7320269372
This is an open-access article distributed under a CC BY license
(Creative Commons Attribution 4.0 International License)
https://creativecommons.org/licenses/by/4.0/

EUS Existence and Uniqueness of Solution
PV Photovoltaic
FF Fractal Fractional
SOC State of Charge
MSE Mean Square Error
RL Riemann-Liouville

1. Introduction

Electric power generation encompasses the conversion of primary energy resources-fossil fuels [1], nuclear reactions, and renewable sources such as solar, wind, hydro, and biomass-into electrical energy through thermodynamic, electrochemical, or photovoltaic processes [2]. The theoretical and applied structures of power generation systems are well studied in the works [3, 4]. Modern systems prioritize efficiency, reliability, and low emissions, integrating advanced turbines, semiconductor power electronics, energy storage, and digital control to balance supply and demand [5]. Grid decarbonization challenges necessitate flexible operation, enhanced transmission infrastructure, and sophisticated forecasting to accommodate variable renewables [6]. Policy mechanisms, market design, and investment in research and deployment shape technological trajectories and determine the pace at which generation portfolios transition toward sustainability over the coming decades globally [7, 8].

Solar-wind hybrid power generation systems integrate Photovoltaic (PV) solar arrays [9] and wind turbines into a power generation system that uses the pair nature of solar and wind resources to make electricity more reliably and efficiently than either source alone [10]. The modern development of renewable energy expanded momentum in the 20th century as concerns about finite fossil fuels, energy security, and environmental degradation grew [11]. Photovoltaics appeared commercially in the 1950s and gradually decreased in cost through materials innovation, economies of scale, and manufacturing advances [12]. Earlier, wind power began as small-scale mechanical windmills, but it expanded in earnest in the 1970s and 1980s [13]. The concept of hybrid renewable systems combining multiple resources to improve reliability grew from early remote-area electrification projects [14]. In many off-grid or weak-grid locations, designers discovered that relying on a single variable resource (only solar or only wind) required substantial energy storage or backup generation. Because solar irradiance and wind speed often show different daily and seasonal patterns, combining them reduces periods of low generation [15]. Pilot hybrid systems-pairing PV and small/medium wind turbines with batteries and sometimes diesel backup-were trialed in island communities, telecom sites, and rural villages from the 1980s onward. As power electronics (inverters and controllers), smart monitoring, and battery technologies matured in the 2000s-2020s, hybrid systems turned into more sophisticated solutions capable of grid-connected operation, dispatch control, and optimized energy management [16].

Solar-wind hybrid systems are versatile and can be designed for multiple reasons: Islands, remote villages, rural public areas, rural institutions, and telecom towers benefit from hybrid systems that reduce or eliminate diesel dependence and improve supply reliability. Community or campus microgrids use hybrid generation plus storage to provide consistent energy that can island during grid outages [17]. Hybrid systems with storage provide a more continuous and predictable injection of renewable energy, improving capacity factors compared to single-source farms. The hybrid systems can lower electricity costs, back against price volatility, and provide suppleness for critical loads [18].

Efficiency and performance in the context of hybrid systems refers to both energy conversion efficiency of each technology (PV module efficiency, wind turbine aerodynamic/mechanical efficiency) and overall system utilization-capacity factor, effective energy given per installed capacity, and reduced limitation or fuel utilization. Wind often rises to highest speed overnight or in different seasons than solar, combined systems achieve higher amount of energy than alone PV or wind farms. For example, while a PV plant may have a capacity factor of 10%–25% depending on location and wind 25%–50% for good sites, a hybrid system can raise average utilization through temporal smoothing. Combining wind turbines and solar arrays can expand total energy generation on a site, improving land-use efficiency compared to separate installations. Modern EMS and inverter systems optimize set points to reduce limitation, perform predictive dispatch using weather forecasts, and balance charging/discharging to minimize losses [19]. However, overall system efficiency also differs

based on design choices (turbine size and spacing, PV tilt and tracking, storage sizing), local resource profiles, and grid integration limitations. Properly fabricated systems tailored to resource patterns and load profiles regularly overtake isolated single-source installations in terms of reliability and levelized cost of electricity [20]. The global energy transition needs rapid, large-scale deployment of low-carbon energy resources. Solar-wind hybrid systems address several critical needs: Solar-wind hybrid systems are justified on multiple borders: Technically, their complementary generation profiles, with wind often peaking when solar output is low and helping in smooth aggregate production, reduce periods of undergeneration and improve reliability while lowering the storage capacity desired to achieve a given level of dispatchability; combining resources and sharing interconnection, control hardware, and site infrastructure also yield economies of scale that reduce capital and management costs per installed kilowatt. Economically, hybrids commonly achieve a lower levelized cost of energy and life-cycle cost than equivalent single-resource projects that need more storage or firming fuel, while offering multiple revenue streams from energy sales, capacity payments, and supplementary services; in off grid applications, and predictable maintenance costs that validate the investment within attractive payback periods [21]. Environmentally and socially, hybrids displace fossil generation, reducing CO_2 and local air pollutants, generate local employment during construction and operation, and deliver resilient and affordable power that supports sectors in rural areas [22].

Structure of the paper: The paper has been organized in five sections and is illustrated in the Figure 1. The first part of the paper is about the introduction of the topic which include the literature review about the energy generation systems, its applications, modeling, simulations, and fractional calculus. The second section is about the mathematical analysis of the model including the Existence and Uniqueness of Solution (EUS), Hyers-Ulam Stability (HUS), and Lipchitz Condition (LC)-criteria. In section 3, a numerical scheme for the model's simulations is illustrated. Section 4 describes the deep learning mechanism for the model. It include neural-networking, Mean Squared Error (MSE), and regression. The final section is the conclusion of the paper which summarize all the findings of the paper and future directions.

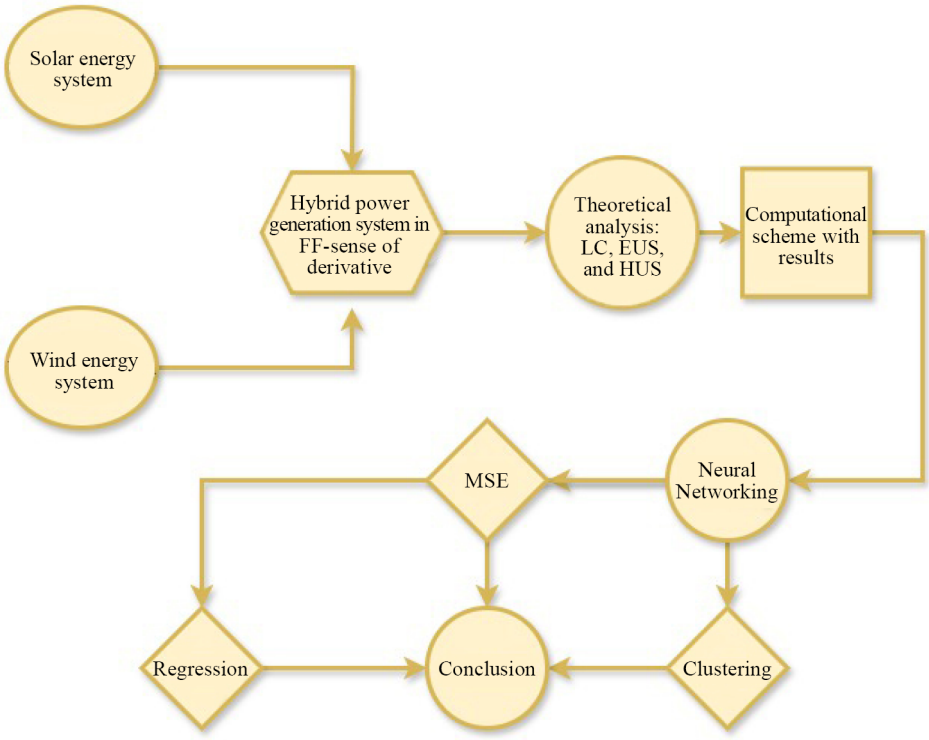


Figure 1. A flowchart of the hybrid power generation system of the article

1.1 *Fractional order modeling of dynamical systems*

Fractional Differential Equations (FDEs) extend integer-order calculus by permitting derivatives of non-integer order, which naturally incorporate memory and hereditary effects into mathematical models. Due to the dependence of fractional derivatives on past values of the function, therefore, FDEs are particularly effective for systems where history influences current behavior-examples include viscoelastic materials that exhibit combined elastic and viscous responses across time scales, anomalous transport in porous media and fluids, and biological processes with long-tail kinetics or subdiffusive motion. Common fractional operators (Riemann-Liouville, Caputo, Grünwald-Letnikov) have different analytical advantages depending on initial and boundary conditions, but analytical solutions are often difficult, so researchers use special functions (e.g., Mittag-Leffler), transform methods, and tailored numerical schemes-finite-difference, finite-element, spectral, and meshless approaches to handle the nonlocal memory terms efficiently. Overall, FDEs frequently outperform integer-order models when describing long-range temporal correlations and anomalous diffusion, making them a powerful operator in modern applied science and engineering [23, 24]. Their flexibility allows for more accurate representations of dynamic systems, especially where classical models are not well useful [25, 26]. In the recent works, the readers can see a bridging role of FDEs between theoretical analysis and computational results in many research articles. For example, Khan et al. [27] considered a cancer model in the framework of discrete fractional derivative and studied the model for both the theoretical and computational works. Ali et al. [28] considered a computational analysis of the nonlinear mathematical system in real world problems. Ravichandran et al. [29] an epidemic model illustrating computer virus dynamics in AB sense of fractional derivative.

Embedding fractal geometry into fractional derivatives produces the fractal-fractional derivative, which generalizes integer and classical fractional calculus [30]. This operator models systems with long-range correlations and irregular, non-differentiable behavior often seen in complex and natural phenomenon [31]. By merging fractal structure with fractional-order dynamics, these derivatives capture both spatial heterogeneity and temporal memory that standard derivatives cannot illustrate [32]. They effectively describe anomalous transport, subdiffusion, and superdiffusion, offering a more precise mathematical description for various phenomena [33]. Consequently, this framework gives a more accurate mathematical presentation for diverse phenomena-ranging from porous media flow [34] and viscoelastic materials to ecological patterns [35] and signal irregularities [36]-where traditional calculus fails in presenting complexity and history-dependent dynamics. Researchers increasingly adopt it to model real-world complex systems accurately [37].

Definition 1 Let $\mathscr{U}(t)$ is continuous in the $(a,\ b)$, then fractional derivative of a, with order γ in RL sense with power law is presented by [30];

$$ {}_aD^{\gamma,\,\beta}\mathscr{U}(t) = \frac{1}{\Gamma(1-\gamma)}\frac{d}{dt^{\beta}}\int_a^t \mathscr{U}(\tau)(t-\tau)^{-\gamma}d\tau, \quad 0<\gamma\leq 1, \tag{1} $$

where

$$ \frac{d\mathscr{U}^{\beta}}{dy} = \lim_{t\to y}\frac{\mathscr{U}(t)-\mathscr{U}(y)}{t^{\beta}-y^{\beta}}. \tag{2} $$

Definition 2 Let $\mathscr{U}(t)$ is a continuous function in the $(a,\ b)$ and Fractional Derivative (FD) of $\mathscr{U}(t)$, of order γ in RL sense with the exponential decay kernel is given by

$$ {}_aD^{\gamma,\,\beta}\mathscr{U}(t) = \frac{M(\gamma)}{1-\gamma}\frac{d}{dt^{\beta}}\int_a^t \mathscr{U}(y)\exp\left(-\frac{t-y}{1-\gamma}\right)dy, \quad 0<\gamma,\ \beta\leq 1. \tag{3} $$

Definition 3 The FD of order γ in RL-sense of $\mathscr{U}(t)$ is given by

$$^{AB}D^{\gamma,\,\beta}\mathscr{U}(t)=\frac{AB(\gamma)}{1-\gamma}\frac{d}{dt^{\beta}}\int_a^t(t-y)^{\gamma-1}\mathscr{U}(y)\,dy,\quad 0\leq\gamma,\,\beta\leq 1,\tag{4}$$

where $AB(\gamma)=1-\gamma+\dfrac{\gamma}{\Gamma(\gamma)}$.

Definition 4 The Fractal-Fractional (FF)-integral of a continuous $\mathscr{U}$ on the interval $(a,\,b)$ of order in γ is given by

$$I^{\gamma,\,\beta}\mathscr{U}(t)=\frac{\beta}{\Gamma(\gamma)}\int_0^t y^{\beta-1}(t-y)^{\gamma-1}\mathscr{U}(y)\,dy.\tag{5}$$

The FF-integral of $\mathscr{U}$ with order in β is given by

$$I^{\gamma,\,\beta}\mathscr{U}(t)=\frac{\beta\gamma}{M(\gamma)}\int_0^t y^{\beta-1}\mathscr{U}(y)\,dy+\frac{\beta(1-\gamma)t^{\beta-1}}{M(\gamma)}\mathscr{U}(t).\tag{6}$$

A Banach space $\mathfrak{B}=\{u\in C([0,\,T]:\mathbb{R})\}$, with a norm $\|u\|=\max_{\mathfrak{t}\in[0,\,T]}|u(\mathfrak{t})|$, is considered for the mathematical analysis of the hybrid system.

1.2 *Artificial intelligence applications in science*

Artificial Intelligence (AI) helps in detecting patterns in large datasets, learning system behavior, and giving more real-time forecasts. Models like Recurrent Neural Networks (RNNs) and Long Short-Term Memory (LSTM) networks are widely applied to time-series forecasting and anomaly detection [38, 39]. AI also helps solve inverse problems by inferring system parameters from experimental observations. Additionally, machine-learning methods automate model selection and finds parameters, and predict errors, enhancing the reliability of dynamical models. These capabilities reduce manual works, accelerate discovery, and enable adaptive modeling as new data is produced. Consequently, AI-driven approaches are increasingly applied in climate modeling, financial prediction, and engineering design, where systems are nonlinear, high-dimensional, and data-rich, making data-driven insights essential for robust decision-making [40, 41], Zika virus dynamics [42], HIV-AIDS simulations [43], contaminants mitigation and transportation analysis [44], sustainable energy with AI [45] risk management and making more efficient, transparent, and resilient solutions can be studied in [46]. For more related results on computational works including the regression analysis can be studied in the references [45–47].

1.3 *Wind-solar hybrid dynamic model*

We consider a five-state model representing the dynamics of a hybrid renewable energy system. The system is governed by the following ordinary differential equations:

$$^{FF}{}_0\mathscr{D}_{\mathfrak{t}}^{\vartheta,\,\varpi}\mathscr{X}_1=-\alpha\mathscr{X}_1+\beta v_w^3-\gamma\mathscr{X}_4,$$

$$^{FF}{}_0\mathscr{D}_{\mathfrak{t}}^{\vartheta,\,\varpi}\mathscr{X}_2=-\delta\mathscr{X}_2+\varepsilon I_s-\eta\mathscr{X}_5,$$

$$^{FF}{}_0\mathscr{D}_{\mathfrak{t}}^{\vartheta,\,\varpi}\mathscr{X}_3=\min\left(\max(\zeta\mathscr{X}_2-\lambda\mathscr{X}_4,\,-0.01),\,0.01\right),$$

$$^{FF}{}_0\mathscr{D}_t^{\vartheta,\varpi}\mathscr{X}_4 = -\mu\mathscr{X}_4 + \nu\mathscr{X}_1 - \rho\mathscr{X}_3,$$

$$^{FF}{}_0\mathscr{D}_t^{\vartheta,\varpi}\mathscr{X}_5 = -\theta\mathscr{X}_5 + \kappa\mathscr{X}_4, \tag{7}$$

where: $\mathscr{X}_1(t)$: Rotor speed (rad/s), $\mathscr{X}_2(t)$: Solar PV voltage (V), $\mathscr{X}_3(t)$: Battery State of Charge (SOC, unitless), $\mathscr{X}_4(t)$: Grid current (A), $\mathscr{X}_5(t)$: DC-link voltage (V), $v_w(t) = 7 + 2\sin(0.05t)$: Time-varying wind speed (m/s), $I_s(t) = \max\left(0, \sin\left(\frac{\pi(t \bmod 24)}{24}\right)\right)$: Normalized solar irradiance. The state variable $\mathscr{X}_3(t)$ (battery SOC) is bounded such that $0 \le \mathscr{X}_3(t) \le 1$. If SOC reaches its upper or lower limit, $\frac{d\mathscr{X}_3}{dt}$ is set to zero to prevent overshooting. The parameters are explained in the Table 1.

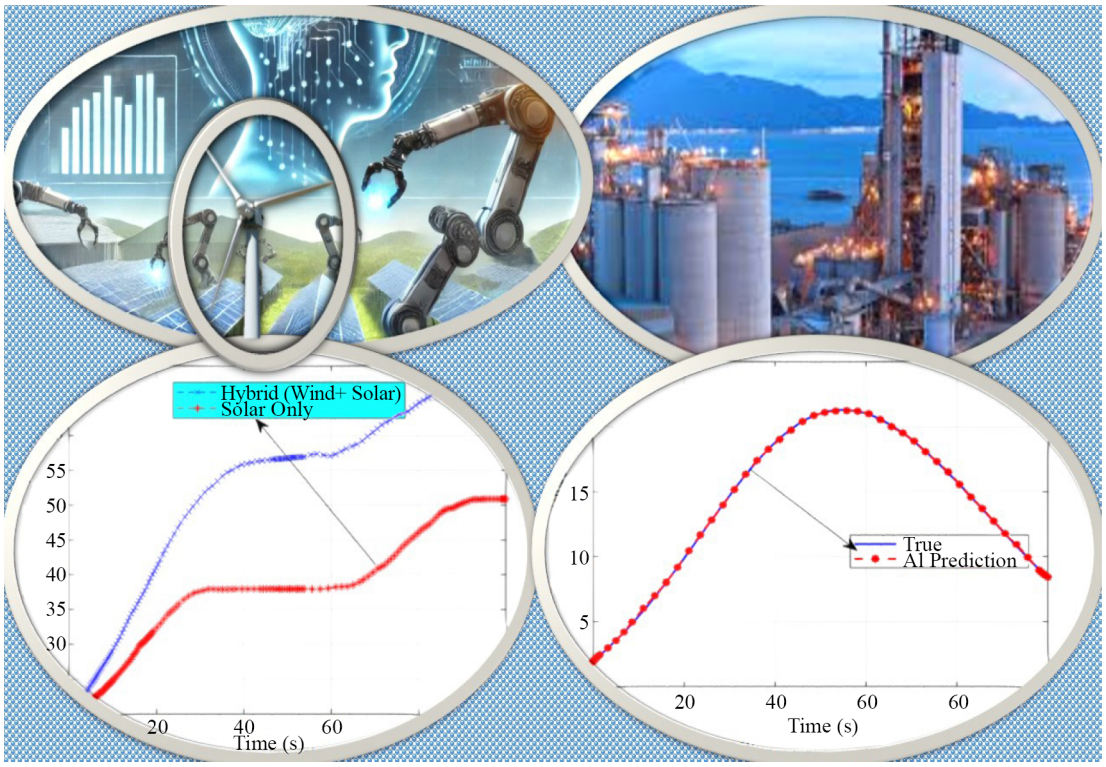


Figure 2. A solar wind hybrid power generation system analysed by mathematical modeling and AI for the green energy dissipation

In Figure 2, we have highlighted the hybrid power generation system and its analysis through AI for the proposed model of the study. In the presented model, wind dynamics influence the system through the time-dependent input $v_w(t) = 7 + 2\sin(0.05t)$, which represents the fluctuating wind speed. This input enters the rotor speed equation via the cubic term βv_w^3, directly impacting the evolution of $\mathscr{X}_1(t)$, the rotor speed. The cubic dependence reflects the physical principle that wind energy captured by turbines scales with the cube of wind speed. Consequently, $v_w(t)$ governs the mechanical input to the system, modulating the rotor's acceleration or deceleration. Thus, wind variability becomes a fundamental driver of energy dynamics within this hybrid model.

Here, we highlight the importance, significance, validation and novelty of the model (7).

• **Importance:** This model has a vital role in understanding the integrated dynamics of wind and solar power generation system. As renewable energy becomes a central part of global power generation, capturing the interplay between environmental inputs and storage systems is essential for designing stable, efficient, and sustainable infrastructure.

• **Validation:** The results produced by the model are consistent with known physical behaviors such as the rise and fall of rotor speed with changing wind energy input, and the saturation of battery state-of-charge under steady solar conditions. These conditions confirm that the model reflects practical engineering behavior and can be further validated against field data from hybrid energy testbeds.

• **Mathematical Feasibility:** The system is constructed from coupled first-order DEs that are well-posed under standard conditions. The use of saturation constraints, such as limiting battery SOC within [0, 1], confirms boundedness and prevents unrealistic numerical divergence. Moreover, all terms are continuously differentiable, making the system flexible to both analytical and numerical methods of solution.

• **Significance:** By simulating multiple cases by changing parametric values, the model provides information into how system performance responds to variation in turbine efficiency or solar conversion rates. This potential to capture sensitivity makes the model particularly useful for optimization studies and controller design in hybrid renewable systems.

• **Impact:** The framework can inform energy policy decisions, assist engineers in developing smarter grid structures, and help academic researchers prototype to improve energy storage. Its versatility gives it to be adapted in a wide range of climatic and geographical areas.

• **Hybrid Superiority:** Unlike standalone solar or wind energy systems, the hybrid system leverages the complementary nature of both energy sources-solar being strongest during the day and wind often with peak at night or under cloudy conditions. This dual-input setup improves overall energy reliability and diminishes dependency on any single environmental source, making the system more resilient and efficient in changing climates.

Table 1. Parameter descriptions and baseline values

Parameter	Description	Value
α	Rotor damping coefficient	0.01
β	Wind energy conversion coefficient	Variable (e.g., 0.0003–0.0042)
γ	Rotor-to-grid interaction factor	0.002
δ	PV voltage decay rate	0.003
ε	Solar irradiance conversion factor	Variable (e.g., 5.0–24.5)
η	DC-link consumption by PV	0.0001
ζ	Charging rate from PV to battery	0.0025
λ	Grid interference on battery SOC	0.0015
ρ	Battery SOC's effect on grid	0.005
θ	DC-link voltage decay rate	0.005
κ	Grid current contribution to DC-link	0.1
μ	Grid current decay rate	0.01
ν	Rotor contribution to grid	0.2

2. Mathematical analysis of the model

Using fixed point approach, we examine the necessary conditions for the solution existence of FF-model (7). For this, we transform the FF-Wind-Solar hybrid power generation system (7) in the following integral form:

$$
\begin{cases}
\mathscr{X}_1(\mathfrak{t}) - \mathscr{X}_1(0) = & \frac{\vartheta\varpi}{\mathfrak{M}(\vartheta)\Gamma\vartheta}\int_0^{\mathfrak{t}} \mathfrak{H}(\mathfrak{t},\ s)(-\alpha\mathscr{X}_1 + \beta v_w^3 - \gamma\mathscr{X}_4)ds + \frac{\varpi(1-\vartheta)t^{\varpi-1}}{\mathfrak{M}(\vartheta)}(-\alpha\mathscr{X}_1 + \beta v_w^3 - \gamma\mathscr{X}_4), \\
\mathscr{X}_2(\mathfrak{t}) - \mathscr{X}_2(0) = & \frac{\vartheta\varpi}{\mathfrak{M}(\vartheta)\Gamma\vartheta}\int_0^{\mathfrak{t}} \mathfrak{H}(\mathfrak{t},\ s)(-\delta\mathscr{X}_2 + \varepsilon I_s - \eta\mathscr{X}_5)ds + \frac{\varpi(1-\vartheta)t^{\varpi-1}}{\mathfrak{M}(\vartheta)}(-\delta\mathscr{X}_2 + \varepsilon I_s - \eta\mathscr{X}_5), \\
\mathscr{X}_3(\mathfrak{t}) - \mathscr{X}_3(0) = & \frac{\vartheta\varpi}{\mathfrak{M}(\vartheta)\Gamma\vartheta}\int_0^{\mathfrak{t}} \mathfrak{H}(\mathfrak{t},\ s)(\min(\max(\zeta\mathscr{X}_2 - \lambda\mathscr{X}_4,\ -0.01),\ 0.01))ds \\
& + \frac{\varpi(1-\vartheta)t^{\varpi-1}}{\mathfrak{M}(\vartheta)}(\min(\max(\zeta\mathscr{X}_2 - \lambda\mathscr{X}_4,\ -0.01),\ 0.01)) \\
\mathscr{X}_4(\mathfrak{t}) - \mathscr{X}_4(0) = & \frac{\vartheta\varpi}{\mathfrak{M}(\vartheta)\Gamma\vartheta}\int_0^{\mathfrak{t}} \mathfrak{H}(\mathfrak{t},\ s)(-\mu\mathscr{X}_4 + \nu\mathscr{X}_1 - \rho\mathscr{X}_3)ds \\
& + \frac{\varpi(1-\vartheta)t^{\varpi-1}}{\mathfrak{M}(\vartheta)}(-\mu\mathscr{X}_4 + \nu\mathscr{X}_1 - \rho\mathscr{X}_3) \\
\mathscr{X}_5(\mathfrak{t}) - \mathscr{X}_5(0) = & \frac{\vartheta\varpi}{\mathfrak{M}(\vartheta)\Gamma\vartheta}\int_0^{\mathfrak{t}} \mathfrak{H}(\mathfrak{t},\ s)(-\theta\mathscr{X}_5 + \kappa\mathscr{X}_4)ds + \frac{\varpi(1-\vartheta)t^{\varpi-1}}{\mathfrak{M}(\vartheta)}(-\theta\mathscr{X}_5 + \kappa\mathscr{X}_4).
\end{cases} \tag{8}
$$

Now, we define some functions $\mathfrak{Q}_i$ and some constants $\rho_i^{\circledast}$, $i\varepsilon N_1^4$, for the main results of the paper.

$$
\begin{cases}
\mathfrak{Q}_1(\mathfrak{t},\ \mathscr{X}_1) = -\alpha\mathscr{X}_1 + \beta v_w^3 - \gamma\mathscr{X}_4, \\
\mathfrak{Q}_2(\mathfrak{t},\ \mathscr{X}_2) = -\delta\mathscr{X}_2 + \varepsilon I_s - \eta\mathscr{X}_5, \\
\mathfrak{Q}_3(\mathfrak{t},\ \mathscr{X}_3) = \min(\max(\zeta\mathscr{X}_2 - \lambda\mathscr{X}_4,\ -0.01),\ 0.01), \\
\mathfrak{Q}_4(\mathfrak{t},\ \mathscr{X}_4) = -\mu\mathscr{X}_4 + \nu\mathscr{X}_1 - \rho\mathscr{X}_3, \\
\mathfrak{Q}_5(\mathfrak{t},\ \mathscr{X}_5) = -\theta\mathscr{X}_5 + \kappa\mathscr{X}_4.
\end{cases} \tag{9}
$$

The mathematical analysis of the FF-Wind-Solar hybrid power generation system necessitates specific assumptions to ensure accurate modeling and reliable results. These foundational assumptions are critical for understanding the interactions and efficiencies within the system's components and overall performance of the model (7).

• $(\mathfrak{A}^{\circledast})$: The continues functions $\mathscr{X}_1$, $\mathscr{X}_2$, $\mathscr{X}_3$, $\mathscr{X}_4$, $\mathscr{X}_5$ and $\mathscr{X}_1^{\circledast}$, $\mathscr{X}_2^{\circledast}$, $\mathscr{X}_3^{\circledast}$, $\mathscr{X}_4^{\circledast}$, $\mathscr{X}_5^{\circledast}$ are contained within $L[0,\ 1]$ to the extent that $\|\mathscr{X}_1\| \le \rho_1^{\circledast}$, $\|\mathscr{X}_2\| \le \rho_2^{\circledast}$, $\|\mathscr{X}_3\| \le \rho_3^{\circledast}$, $\|\mathscr{X}_4\| \le \rho_4^{\circledast}$, $\|\mathscr{X}_5\| \le \rho_5^{\circledast}$ for $\rho_1^{\circledast}$, $\rho_2^{\circledast}$, $\ldots$, $\rho_5^{\circledast} > 0$ and constants.

Theorem 1 The kernals $\mathfrak{Q}_i$ are satisfying Lipchitz conditions if the assumptions $(\mathfrak{A}^{\circledast})$, is satisfied and $\phi_i < 1$, for $i \in N_1^5$.

Proof. First, we consider $\mathfrak{Q}_1(\mathfrak{t},\ \mathfrak{T})$ for the Lipschitz condition. We proceed for this below:

$$
\|\mathfrak{Q}_1(\mathfrak{t},\ \mathfrak{E}) - \mathfrak{Q}_1(\mathfrak{t},\ \mathfrak{E}^{\circledast})\| \|(-\beta\mathfrak{A}\mathfrak{E} + \omega\mathfrak{R}) - (-\beta\mathfrak{A}\mathfrak{E}^{\circledast} + \omega\mathfrak{R}))\| \beta\|\mathfrak{A}\| \|\mathfrak{E} - \mathfrak{E}^{\circledast}\| \le \beta\rho_5^{\circledast}\|\mathfrak{A}\| \|\mathfrak{E} - \mathfrak{E}^{\circledast}\|,
$$

where $\phi_1 = \beta\rho_5^{\circledast}$. Hence, the LC criteria for $\mathfrak{Q}_1$ holds true, as $\rho_1 < 1$. For $\mathfrak{Q}_2(\mathfrak{t},\ \mathfrak{P})$, we get $\phi_2 = \sigma$, where $\rho_2 < 1$, which implies that $\mathfrak{Q}_2(\mathfrak{t},\ \mathfrak{P})$ also satisifies the LC requirement. Similarly, we have $\rho_3 = \rho$, $\rho_4 = \omega$, and $\rho_5 = \eta$. Since, $\rho_i < 1$, for all $i = 1,\ 2,\ \ldots,\ 5$, therefore, the $\mathfrak{Q}_i$, for $i,\ 3,\ 4,\ 5$, are also holding the LC criteria. This completes the proof. □

Theorem 2 The condition $(\mathfrak{A}^{\circledast})$, ensures the solution existence for the FF-Wind-Solar hybrid power generation system (7) and is further implying the mathematical feasibility of the model.

Theorem 3 The assumption $(\mathfrak{A}^{\circledast})$, ensures the solution uniqueness for the FF-Wind-Solar hybrid power generation system (7) and is further validating the mathematical structure of the model.

Theorem 4 The assumption $(\mathfrak{A}^{\circledast})$, guarantees the is Hyers-Ulam stability of the solution for the FF-Wind-Solar hybrid power generation system (7) and is further implying the tolerance of the dynamical system against the small perturbation in the initial stage.

Theorem 5 The assumption $(\mathfrak{A}^{\circledast})$, ensures the is generalized Hyers-Ulam stability of solution for the FF-Wind-Solar hybrid power generation system (7) and is further implying that a slight variation in the solutions is not causing to a larger deviation.

Note: As the article is focuses on the AI-based deep learning of the Wind-Solar hybrid power generation system (7), therefore the mathematical proof is omitted in this work. However, we highlight the procedure for the proofs in literature [27–29, 47].

3. Numerical scheme

The computational iterative loop for the simulation of the FF-Wind-Solar hybrid power generation system (7) is illustrated here. Starting from: ${}^{FFM}{}_0D_{\mathfrak{t}}^{\varsigma_1,\ \varsigma_2}{}_m\mathfrak{V}(\mathfrak{t}) = \rho(\mathfrak{t},\ {}_m\mathfrak{V}(\mathfrak{t}))R$, where ${}_m\mathfrak{V}(0) = {}_m\mathfrak{V}_0$. This is equivalent to:

$$ {}_0^C D_{\mathfrak{t}}^{\varsigma_1}[{}_m\mathfrak{V}](\mathfrak{t}) = \varsigma_2 t^{\varsigma_2 - 1}\rho(\mathfrak{t},\ {}_m\mathfrak{V}(\mathfrak{t})). \tag{10}$$

Applying Riemann-Integral, we have

$$ {}_m\mathfrak{V}(\mathfrak{t}) = {}_m\mathfrak{V}(0) + \frac{\varsigma_1}{\Gamma(\varsigma_1)}\int_0^{\mathfrak{t}} (\mathfrak{t}-\xi)^{\varsigma_1 - 1}\xi^{\varsigma_2 - 1}\rho(\xi,\ {}_m\mathfrak{V}(\xi))d\xi. \tag{11}$$

Replacing $(\mathfrak{t})$ by t_{n+1} we have

$$ {}_m\mathfrak{V}^{n+1} = {}_m\mathfrak{V}(0) + \frac{\varsigma_1}{\Gamma(\varsigma_1)}\int_0^{\mathfrak{t}_{n+1}} (\mathfrak{t}_{n+1}-\xi)^{\varsigma_1 - 1}\xi^{\varsigma_2 - 1}\rho(\xi,\ {}_m\mathfrak{V}(\xi))d\xi. \tag{12}$$

Using two-step Lagrange Polynomial to integrate (12), we get

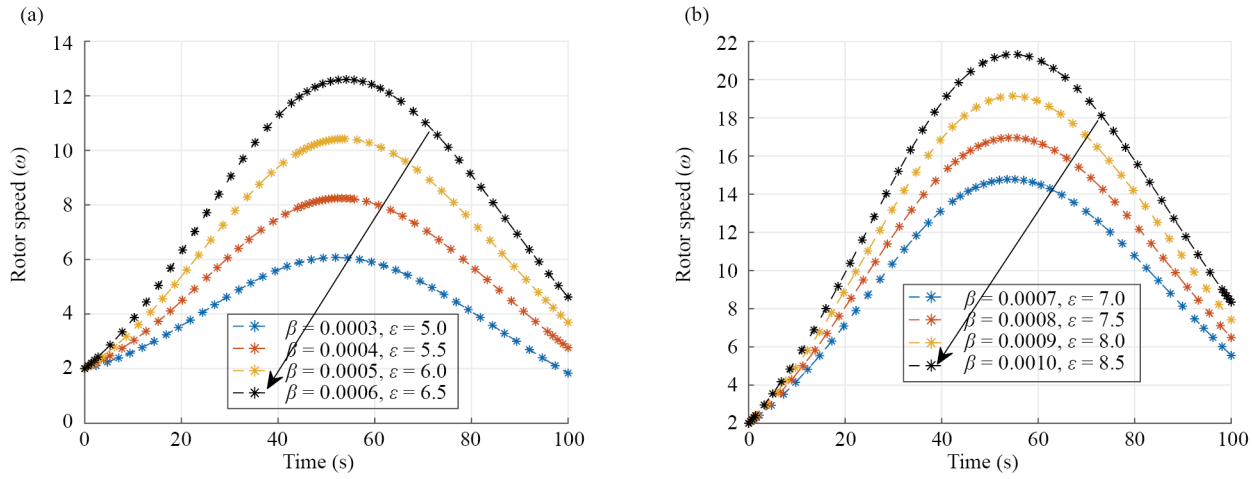
$$ \xi^{\varsigma_2 - 1}\rho(\xi,\ {}_m\mathfrak{V}(\xi)) = \frac{\xi - t_{j-1}}{t_j - t_{j-1}}t_j^{\varsigma_2 - 1}\rho(\xi_j,\ {}_m\mathfrak{V}(\xi_j)) - \frac{\xi - t_j}{t_j - t_{j-1}}t_{j-1}^{\varsigma_2 - 1}\rho(\xi_{j-1},\ {}_m\mathfrak{V}(\xi_{j-1})).$$

The integration yield, the following scheme

$$
{}_m\mathfrak{V}^{n+1} = {}_m\mathfrak{V}(0) + \frac{\varsigma_2 h^{\varsigma_1}}{\Gamma(\theta_1+2)}\left[\sum_{j=0}^{n} t_j^{\varsigma_2-1}\Omega_j\big((n+1-j)^{\varsigma_1}(\varsigma_1+n+2-j)-(n-j)^{\varsigma_1}(2\varsigma_1-j+n+2)\big)\right.
$$

$$
\left. -\sum_{j=0}^{n} t_{j-1}^{\varsigma_2-1}\rho_{j-1}\big((n+1-j)^{\varsigma_1+1}-(n-j)^{\varsigma_1}(\varsigma_1-j+n+1)\big)\right]. \tag{13}
$$

The solution trajectories, and neural networks are trained to forecast $\mathfrak{E}(t)$, $\mathfrak{C}(t)$, and $\mathfrak{A}(t)$ for $\beta = 0.001$.



(a) The Rotor speed (rad/s) developed by the Wind-Solar hybrid power generation system of the model (7) for the variant β and ε as case 1

(b) The Rotor speed (rad/s) developed by the Wind-Solar hybrid power generation system of the model (7) for the variant β and ε as case 2

Figure 3. The Rotor speed (rad/s) dynamics of the Wind-Solar hybrid power generation system of the model (7) for the case 1: $\beta = 0.0003, 0.0004, 0.0005, 0.0006$ and $\varepsilon = 5.0, 5.5, 6.0, 6.5$, and case: $\beta = 0.0007, 0.0008, 0.0009, 0.0010$ and $\varepsilon = 7.0, 7.5, 8.0, 8.5$

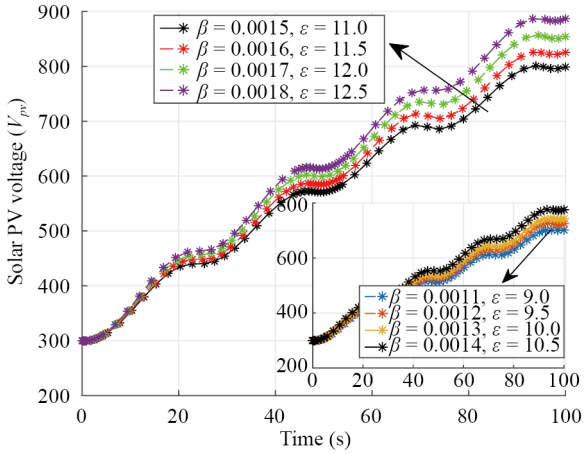
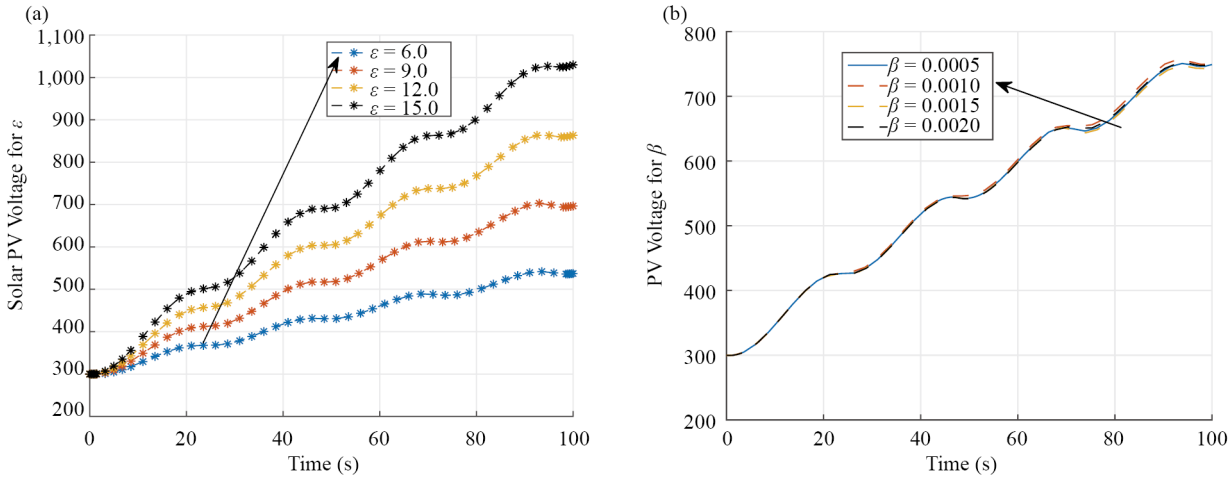


Figure 4. Solar PV voltage dynamics of the hybrid power generation system (7) for the variant $\beta = 0.0011, 0.0012, \ldots, 0.0018$, and $\varepsilon = 9, 9.5, \ldots, 12.5$

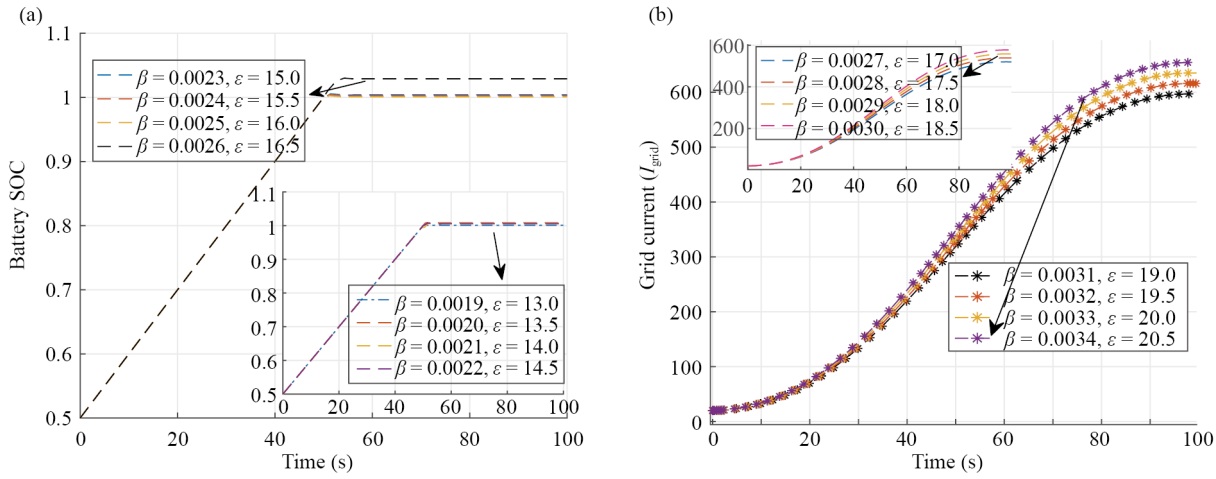
In Figure 3, the Rotor speed dynamics $\mathscr{X}_1$ is illustrated driven by the wind-solar hybrid dynamical system (7) for the case 1: $\beta = 0.0003, 0.0004, 0.0005, 0.0006$ and $\varepsilon = 5.0, 5.5, 6.0, 6.5$, and case: $\beta = 0.0007, 0.0008, 0.0009, 0.0010$ and $\varepsilon = 7.0, 7.5, 8.0, 8.5$. The case 1 is considered in the Figure 3a while the case 2 is illustrated in the Figure 3b. It is observed that for the larger β and ε, the Rotor speed is more than for the smaller values of the parameters.

The solar photovoltaic voltage dynamics $\mathscr{X}_2$ of the hybrid power generation dynamical system is explained in the Figures 4 and 5 for different values of $\beta = 0.0011,\ 0.0012,\ \ldots,\ 0.0018$, and $\varepsilon = 9,\ 9.5,\ \ldots,\ 12.5$. It is observed that for the larger β and ε, there is a higher voltage generation of the system in comparison to the smaller values. The state of charge (Battery SOC) $\mathscr{X}_3$ is illustrated in the Figure 6. We have also given the grid current dynamics of the hybrid system in the figure. The two dynamics of the model are illustrated in Figure 6a and 6b. In Figure 6a, we observed that



Solar PV voltage for ε Solar PV voltage for β

Figure 5. Solar PV voltage dynamics under the hybrid system of Wind-Solar power generation system (7)



State of charge of the battery $\mathscr{X}_3$ measured by the dynamical system of hybrid power generation system (7)

Grid current $\mathscr{X}_4$ dynamics by the hybrid power generation system (7)

Figure 6. Illustrative figures for the state of charge of the battery and grid current dynamics of the Fractal-fractional power generation dynamical system (7)

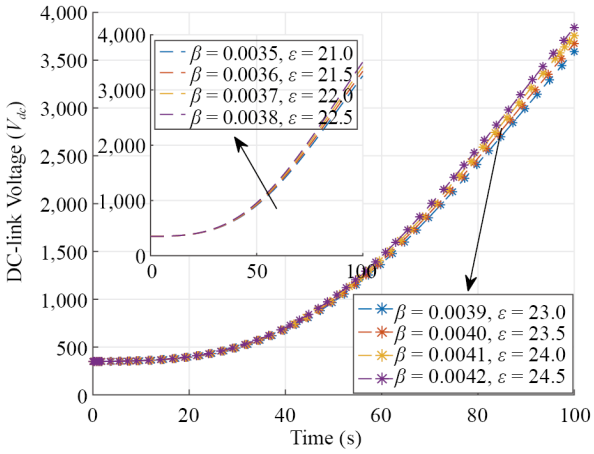


Figure 7. Re-secured population of systems of different values of β of the FF-Wind-Solar hybrid power generation system (7)

In Figure 7, the DC voltage generated by the hybrid system given by the model (7) is illustrated for the different $\beta = 0.0035 - 0.0042,\ \varepsilon = 21 - 24.5$.

4. Deep learning analysis

Here, we explain the training of an AI model to learn an optimal mapping (g) that projects input data (χ) to outputs $(\mathfrak{Y})$ by minimizing a loss function $(L(g(\chi),\ \mathfrak{Y}))$ through systematic adjustment of model parameters; this procedure is demonstrated for the complex neural dynamics of a wind-solar hybrid mechanism model. A widely used optimization method is gradient descent, which iteratively updates parameters according to

$$\theta^{(t+1)};=;\theta^{(t)};-;\eta_0,\ \nabla L!\left(\theta^{(t)}\right), \tag{14}$$

where (θ) represents the model parameters (weights and biases), (η_0) is the learning rate, and $(\nabla L(\theta))$ is the gradient of the loss with respect to the parameters. The choice of (η_0) affects convergence: an excessively large learning rate can cause instability or divergence, whereas an overly small value leads to slow increase and prolonged training. In practice, training commonly means learning-rate schedules, adaptive optimizers (e.g., Adam, RMSprop), gradient clipping, weight regularization, early stopping, and mini-batch updates to stabilize training, accelerate convergence, and enhance generalization. These techniques help the network capture multi-scale temporal features and long-memory effects inherent in the fluctuation of weathers and wind flow.

In Figure 6a we present training results for the deep-learning reconstruction of the wind-solar hybrid power generation model in equation (7) using a fractional-order (FF $= 0.98$), illustrating the model fit, convergence behaviour, and the network's ability to reproduce the system's complex temporal dynamics.

A loss function quantifies the discrepancy between predicted and actual values. The MSE is calculated using the formula: $MSE = \frac{1}{n}\sum_{i=1}^{n}(\mathfrak{V}_i - \hat{\mathfrak{V}}_i)^2$, where $\hat{\mathfrak{V}}_i$ represents the predicted values. To evaluate the model's ability to generalize to new, unseen data, validation performance is measured. Cross-validation methods were employed to successfully group the training data into distinct training and validation sets. The optimal validation performance recorded at the 759th epoch, yielding a minimum MSE of 1.1547, at which point the simulations were concluded successfully.

4.1 *Neural networking*

A data of 600 points was considered for the neural networking. 300 data points were considered as training points while 300 as the targets. The data was trained as per Levenberg-Marquardt techniques. In the Figure 8, the neural networking tabular description is presented for the FF-Wind-Solar hybrid power generation system breach and re-securing dynamical system (7). Here, we have shown that the system has executed a total of 1,000 epochs in time 00:02:50. The performance was considered the initial value 6.1×10^{3} which stopped at 2.37×10^{-9}. The gradient was initially considered 9.43×10^{3} but it stopped at 1.92×10^{-4}. μ at epoch 0 was 0.001 and stopped at 1×10^{-08}. The training of the data was carried out by the help of the Levenberg-Marquardt principle and mean square error was also calculated.

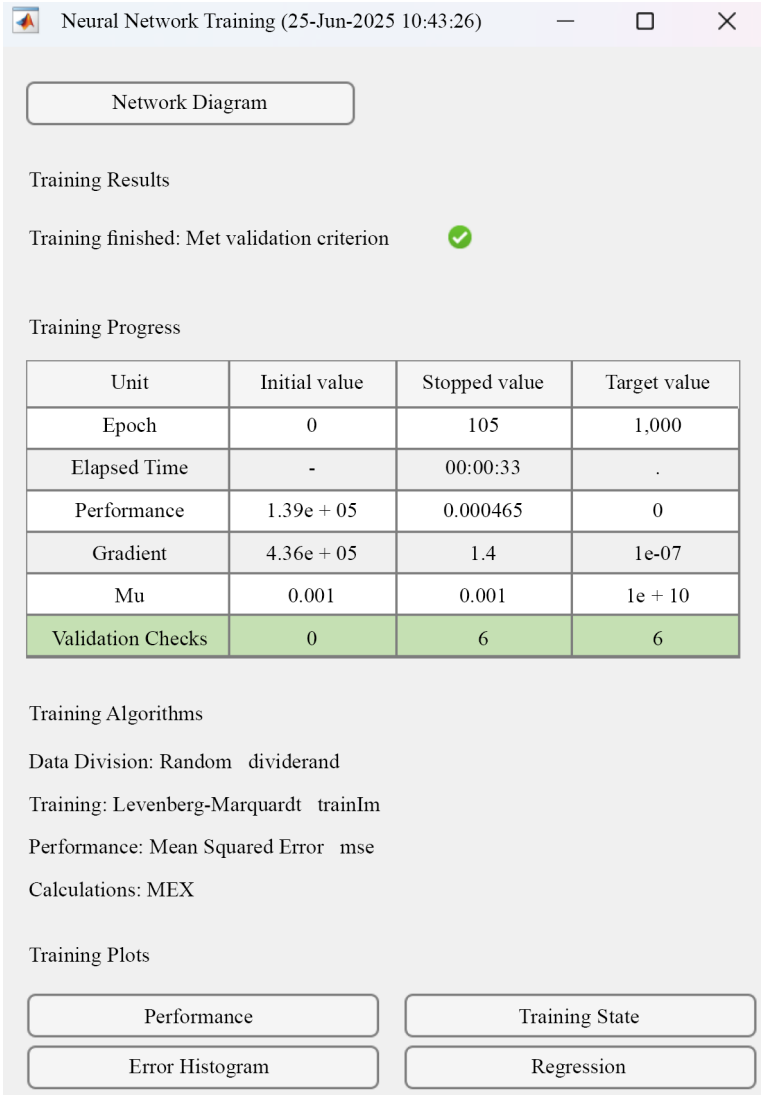


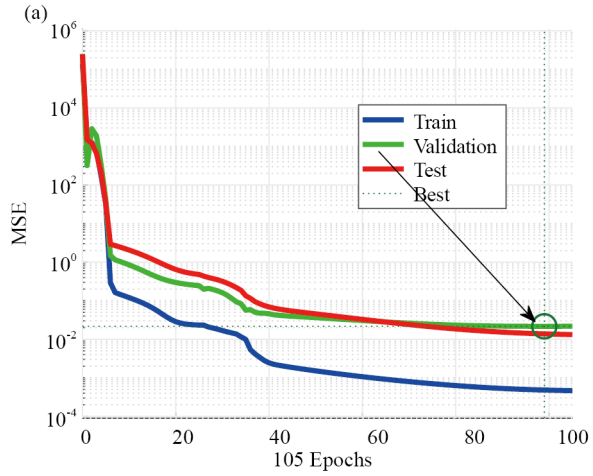
Figure 8. The deep learning analysis of the Wind-Solar hybrid power generation system, as described in (7), employs the Levenberg-Marquardt method at FF-orders of 0.980.980.98. This approach evaluates performance, training conditions, error distribution, and regression estimates to optimize system efficiency and accuracy in future predictions

4.2 *MSE mechanism*

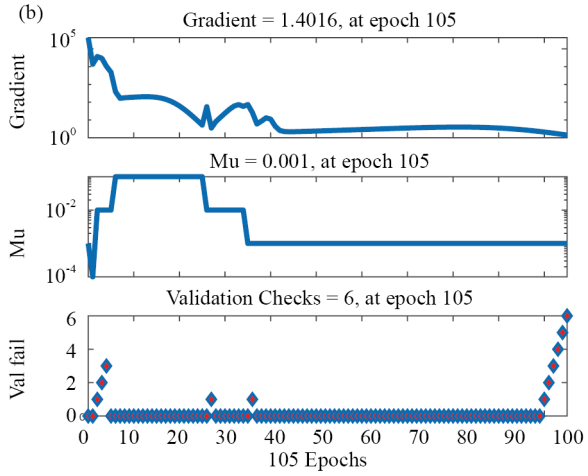
This section presents an AI-driven analysis of the MSE computed from the data produced by model (7). The MSE provides a concise measure of average squared deviation between observed and predicted values and is used here to quantify model precision, guide hyperparameter tuning, and compare alternative architectures. We also explain practical considerations such as normalization of input data, the effect of outliers, use of cross-validation to estimate generalization error, and reporting confidence intervals or bootstrap estimates for robustness. Together, these novel techniques help MSE reliably reflects the predictive performance and stability of the computational model.

$$\text{MSE} = \frac{1}{m}\sum_{i=1}^{m}\left(\mathfrak{V}_i - \hat{\mathfrak{V}}_i\right)^2,$$

where $\mathfrak{V}_i$ represents the true (observed) value, $\hat{\mathfrak{V}}_i$ denotes the model prediction, and m is the total number of data points used in the analysis. A smaller MSE shows higher model precision. The BVF highlights the ideal balance where the model operates successfully on new data, preventing both overfitting and underfitting, thus ensuring strong generalization. This balance is important for building consistent projecting systems that maintain accuracy beyond the training set.



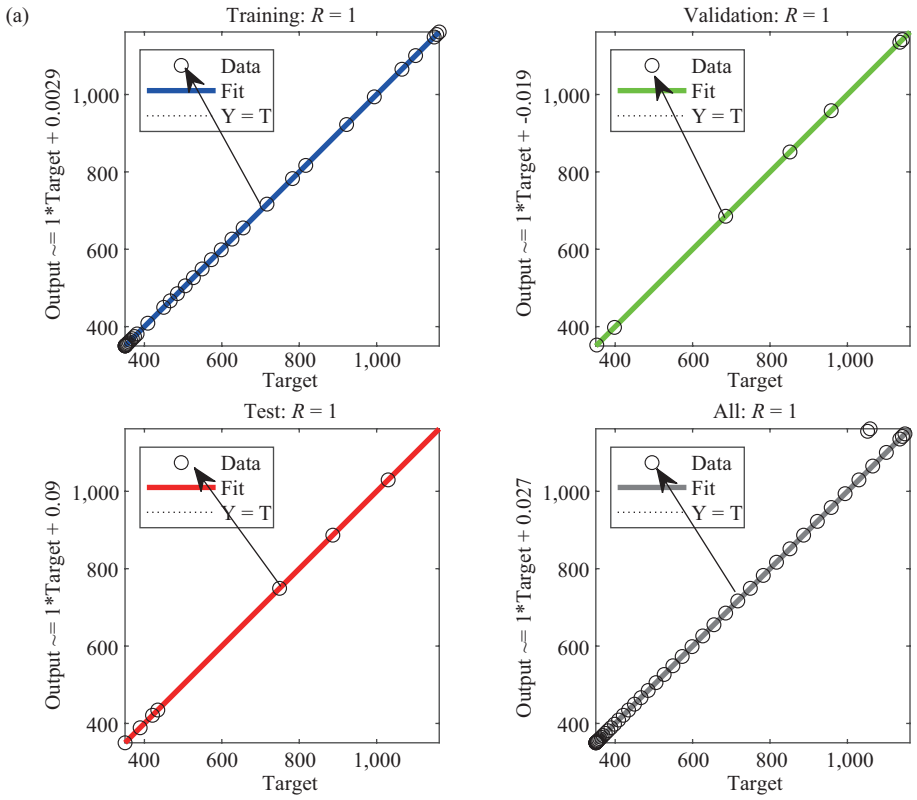
Training the models data for the deep learning based analysis of FF-Wind-Solar hybrid power generation system (7)



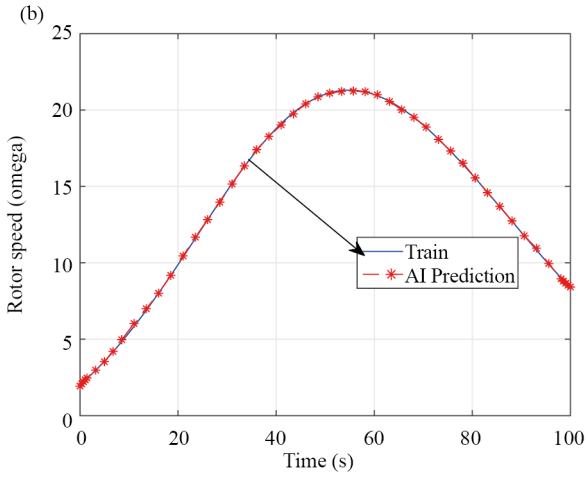
Mean Square Error for the intricate FF-Wind-Solar hybrid power generation system (7) for the FF-orders 0.98

Figure 9. Training the models data for the deep learning based analysis of FF-Wind-Solar hybrid power generation system (7) and the best validation performance 2.3767×10^{-07} at 1,000 epoch

In Figure 9, the training of simulation data for the FF-Wind-Solar hybrid power generation system (7) and the best performance of the computational technique are illustrated. These aspects are highlighted in two subfigures. In the Figure 9a, the gradient of the data is shown as 1.9194×10^{-4} at 1,000 epoch, the corresponding $\mu = 1 \times 10^{-8}$. The best validation performance of the data for the FF-Wind-Solar hybrid power generation system (7) is observed as 2.3767×10^{-7} at epoch 1,000. For the best validation, the system has considered three data scales. Including the training data set, with validation and test. These are simultaneously plotted with best and the trained data has obtained the best validation performance as 2.3767×10^{-7} at 1,000 epoch, given in the Figure 9b. AI based regression analysis of the solar-wind system for the motor speed are expressed in Figure 10a and 10b, respectively.



The evaluation of FF-Wind-Solar hybrid power generation system (7) for the Regression



Error histogram of the FF-Wind-Solar hybrid power generation system (7)

Figure 10. Deep learning results for Wind-Solar hybrid power generation system (7) for the FF-orders 0.98 by Levenberg-Marquardt techniques for regression and error estimations

4.3 *Regression of the data*

Regression analysis is employed to recognize and quantify relationships between variables in a dataset. It helps predict outcomes, understand trends, and determine how independent variables control a dependent variable. This is extensively used

in research, economics, and science for precise modelling and decision-making based on observed data. Linear and logistic regression techniques are used for this work. It is mathematically determined with the following formulation:

$$\mathfrak{Z} = \vartheta_0^{\circledast} + \vartheta_1^{\circledast}\mathfrak{V}_1 + \vartheta_2^{\circledast}\mathfrak{V}_2 + \cdots + \vartheta_n^{\circledast}\mathfrak{V}_n + \xi^{\circledast}, \tag{15}$$

here $\xi\circledast$ is for random error. The $\gamma^{\circledast}$ is produced by the following optimization procedure:

$$\hat{\gamma^{\circledast}} = (\mathfrak{V}^T\mathfrak{V})^{-1}\mathfrak{V}^T\mathfrak{Z}. \tag{16}$$

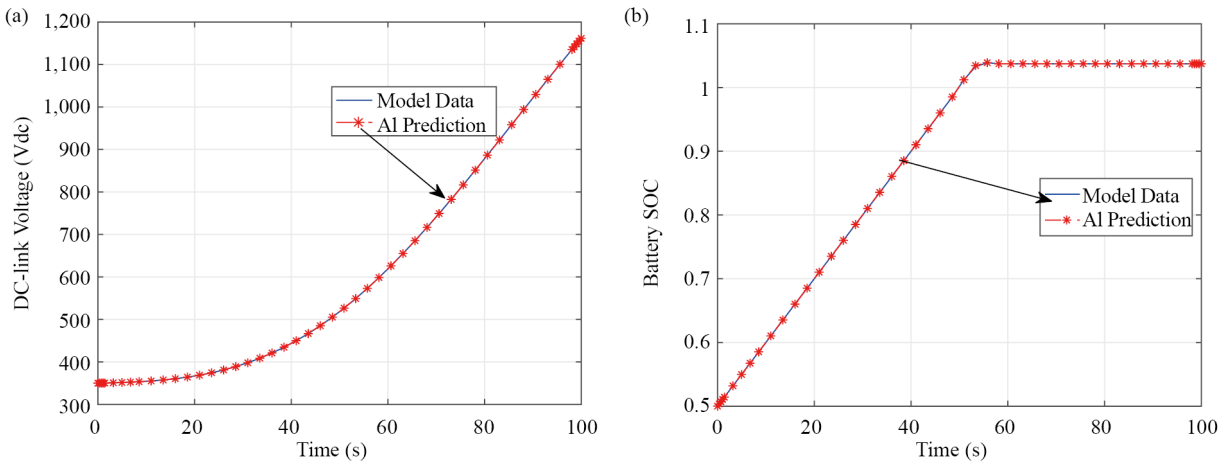
And logistic-regression is evaluated by the following formulation:

$$P(\mathfrak{Z}=1|\mathfrak{V}) = \frac{1}{1+e^{-(\gamma_0^{\circledast}+\vartheta_1^{\circledast}\mathfrak{V}_1+\ldots+\gamma_n^{\circledast}\mathfrak{V}_n)}} \tag{17}$$

This function, guarantees output probabilities in between 0, to 1. We use for error histogram:

$$E_i = {}_m\mathfrak{V}_i - m\hat{\mathfrak{V}}_i, \tag{18}$$

where, ${}_m\mathfrak{V}_i$ are the actual values of the membrane potential while $m\hat{\mathfrak{V}}_i$ are the predicted values. One can see some more relevant works on the topic in [46]. Our analysis has presented regression analysis for the presumed and error estimation in the computational data of the FF-Wind-Solar hybrid power generation system (7) in Figure 11 is illustrated. It is shown in the Figure 11a, that the Regression for the training data set with the $Out\,put \approx 1 * Target + 1.4 \times 10^{-6}$ is 1. The output for the validation is studied with the help of the relationship $Out\,put \approx 1 * Target - 3.3 \times 10^{-5}$. For the testing data, the regression is 1 and is evaluated with the formulation $Out\,put \approx 1 * Target - 1.7 \times 10^{-4}$. All the data sets are jointly studied for the regression in the against the target with the relation $out\,put \approx 1 * Target - 2.4 \times 10^{-5}$ as shown in the Figure 11a.



The evaluation of FF-Wind-Solar hybrid power generation system (7) for the Regression

Error histogram of the FF-Wind-Solar hybrid power generation system (7)

Figure 11. Deep learning results for FF-Wind-Solar hybrid power generation system (7) for the FF-orders 0.98 by Levenberg-Marquardt techniques for regression and error estimations

4.4 *Clustering*

Clustering is a core unsupervised learning technique in data science and machine learning, designed to identify structure within datasets by grouping similar data points. Its primary objective is to divide a set of objects into subsets (clusters) where objects within the same group share high similarity, and those in different groups are dissimilar. Clustering plays a crucial role in various scientific domains, including genomics, image analysis, market segmentation, and renewable energy modeling.

One of the most widely used algorithms is *k-means clustering*, which partitions n data points $\{x_1, x_2, \ldots, x_n\}$ into k disjoint clusters $\{C_1, C_2, \ldots, C_k\}$ by minimizing the intra-cluster variance:

$$\min_{C_1, \ldots, C_k} \sum_{i=1}^{k} \sum_{x \in C_i} \|x - \mu_i\|^2,$$

where μ_i is the centroid of cluster C_i. In contrast, density-based methods like DBSCAN detect clusters of arbitrary shapes without needing the number of clusters in advance.

Clustering algorithms vary in complexity, assumptions, and performance, depending on the structure of the data. Accurate clustering enhances understanding of latent patterns, supports feature extraction, and serves as a preprocessing step in predictive modeling and intelligent decision systems.

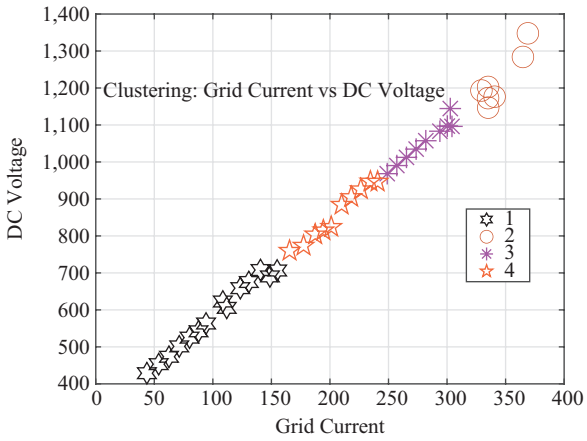


Figure 12. Deep learning analysis of the FF-Wind-Solar hybrid power generation system (7) for the FF-orders 0.98 using Levenberg-Marquardt procedure for the performance, training state, error histogram and regression estimations

In Figure 12, The clustering plot titled "Clustering: Grid Current vs DC Voltage" visually classifies the dynamic behavior of the wind-solar hybrid system under 40 different parametric conditions using k-means clustering technique is illustrated. The X-axis represents grid current, while the Y-axis shows the corresponding DC-link voltage. Four distinct clusters are observed, each marked with a different color and symbol. The separation among clusters indicates that changes in wind and solar input parameters significantly influence the electrical behavior of the system. Cluster 1 represents low power regions, while Clusters 3 and 4 group high-performance operating points, supporting parameter-based optimization and controller tuning strategies.

He Figure 13 illustrates how clustering algorithms partition data into distinct groups based on similarity. Each cluster contains data points with high intra-group cohesion and low inter-group similarity. Such visual separation validates the effectiveness of the clustering method used. This segmentation enables insightful analysis, pattern detection, and data-driven decision-making in complex multidimensional systems like hybrid energy models.

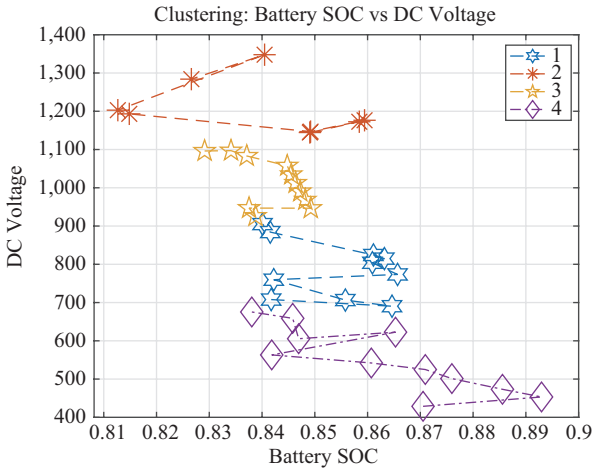


Figure 13. Deep learning analysis of the FF-Wind-Solar hybrid power generation system (7) for the FF-orders 0.98 using Levenberg-Marquardt procedure for the performance, training state, error histogram and regression estimations

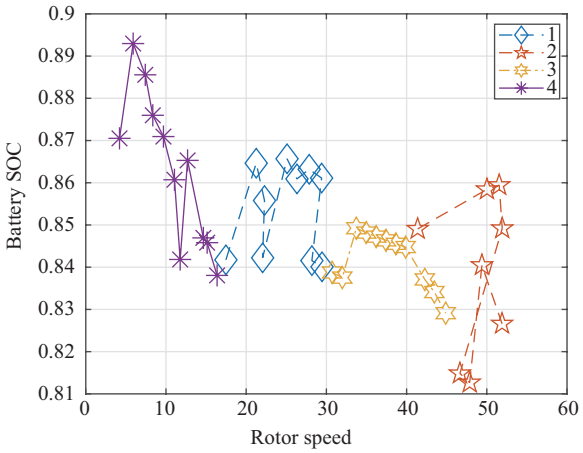


Figure 14. Deep learning analysis of the FF-Wind-Solar hybrid power generation system (7) for the FF-orders 0.98 using Levenberg-Marquardt procedure for the performance, training state, error histogram and regression estimations

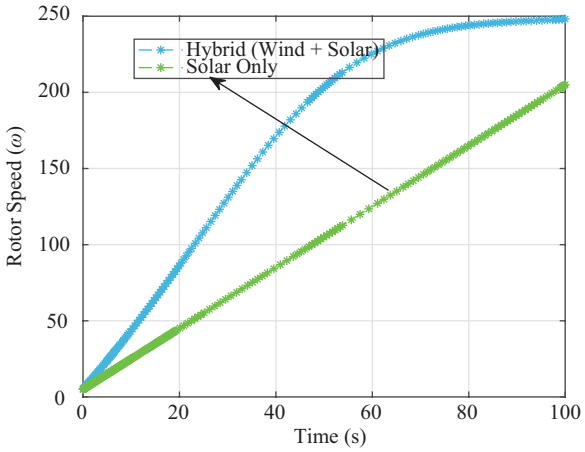


Figure 15. Rotor speed developed by the hybrid system and solar alone

In Figure 14, This clustering plot analyzes the relationship between rotor speed and battery SOC in the hybrid wind-solar energy system under various parameter configurations. The X-axis represents rotor speed (rad/s), while the Y-axis denotes SOC values. The system data has been grouped into four distinct clusters, each with a unique marker and color, highlighting operational similarities within each group. The spread of clusters reveals nonlinear behavior in battery response to the variation in rotor dynamics. Higher SOC levels tend to occur at lower rotor speeds (Cluster 4), indicating efficient energy capture, while wider SOC fluctuations appear at higher rotor speeds (Cluster 2 and 3).

In Figure 15, the computational results for the rotor's speed for the hybrid system of wind and solar is compared with that of the solar alone. It is observed that the speed for the hybrid speed is much higher than the solar alone.

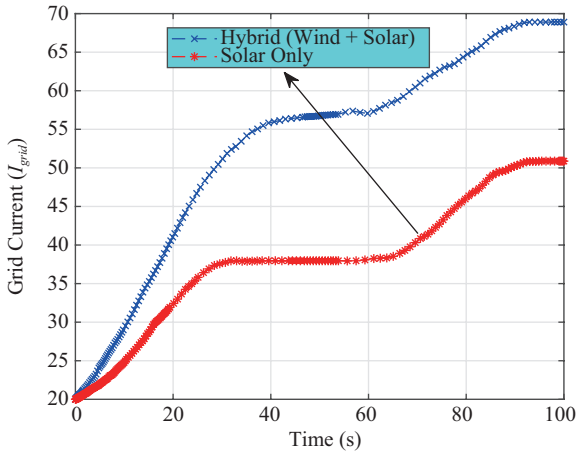


Figure 16. Grid current generated by the hybrid system and solar alone

In the Figure 16, the Grid current is analysed for and compared for both the systems. It is observed that the hybrid system is generating higher level of the current in comparison to the solar system alone.

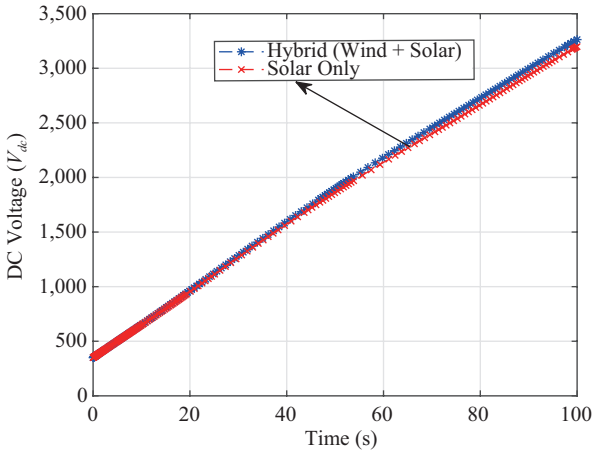


Figure 17. DC voltage generated by the hybrid system in comparison with the solar system alone

In the Figure 17, it is observed that the hybrid system is capable of more DC-voltage generation in comparison to the solar system alone.

5. Conclusions

This paper highlights the importance of hybrid systems in power generation and confirm that the hybrid is escalating the electricity production and is helping in the maintenance of the power in weather fluctuations and light variation. For this, we considered a wind-solar hybrid power generation model in the FF-sense of derivative with five variables including; $\mathscr{X}_1(t)$: Rotor speed (rad/s), $\mathscr{X}_2(t)$: Solar PV voltage (V), $\mathscr{X}_3(t)$: Battery state of charge (SOC, unitless), $\mathscr{X}_4(t)$: Grid current (A), $\mathscr{X}_5(t)$: DC-link voltage (V), $v_w(t) = 7 + 2\sin(0.05t)$: Time-varying wind speed (m/s), $I_s(t) = \max\left(0, \sin\left(\frac{\pi(t \bmod 24)}{24}\right)\right)$: Normalized solar irradiance. The state variable $\mathscr{X}_3(t)$ (battery SOC) is bounded such that $0 \leq \mathscr{X}_3(t) \leq 1$. The model is first mathematically analysed for the existence of solutions and stability results. After these, we established a computational scheme for the numerical simulations and the model is solved for the FF orders 0.98. The simulations indicated that the DC voltage produced by the hybrid system is much better than the solar alone. Also, the grid current for the hybrid system is better than the solar alone as a source of generation. Besides these, the rotor speed was analysed and found much faster than the solar alone. Cluster analysis of these results were made for the DC voltage, battery SOC. It was also observed that the model's data were well fitted to the prediction results and were affirmed by the artificial intelligence. For the training, validation and test results, we found that the regression was 1. These results confirmed the validity of the hybrid systems and the following recommendations are suggested:

• **Integration into Smart Grids:** Given the stability and efficiency of the hybrid wind-solar model under fluctuating weather conditions, it is recommended to integrate such systems into smart grids, particularly in regions with intermittent renewable energy resources.

• **Battery Management Optimization:** The bounded behavior and performance of the battery SOC suggest that improved battery management strategies-leveraging AI prediction models-can further enhance energy storage and dispatch reliability.

• **Deployment in Remote or Off-Grid Areas:** The enhanced rotor speed, DC-link voltage, and grid current indicate that hybrid systems are ideal for deployment in remote or off-grid locations where consistent power supply is critical and standalone solar systems are insufficient.

• **Adoption of Fractional-Order Modeling in System Design:** The successful use of the FF-sense derivative and order 0.98 in simulating dynamic system behavior shows that fractional-order modeling should be further adopted in the design and analysis of renewable energy systems for more accurate and stable predictions. The model can be reconstructed for the control of power loss and improvement of the energy generation by the help of modified ABC and stochastic approaches.

Author contributions

H.K.: Writing original draft, Investigation, Conceptualization. H.B.A., J.A: Investigation, Review manuscript, Editing. R.T, R.A: Validated the results, Review manuscript, Conceptualization, Software.

Acknowledgement

H.K, J.A, would like to thank Prince Sultan University for their financial support to this research work and its publication charges (APC). W.F.A. extends her appreciation to Princess Nourah bint Abdulrahman University Researchers Supporting Project number (PNURSP2026R371), Princess Nourah bint Abdulrahman University, Riyadh, Saudi ArArabia.

Data availability

All data generated or analysed during this study are included in this published article.

Conflict of interest

The authors declare no competing financial interest.

References

[1] Weedy BM, Cory BJ, Jenkins N, Ekanayake JB, Strbac G. *Electric Power Systems*. Hoboken, NJ: John Wiley & Sons; 2012.

[2] Beér JM. High efficiency electric power generation: The environmental role. *Progress in Energy and Combustion Science*. 2007; 33(2): 107–134. Available from: https://doi.org/10.1016/j.pecs.2006.08.002.

[3] Singh SN. *Electric Power Generation: Transmission and Distribution*. New Delhi: PHI Learning Pvt. Ltd.; 2008.

[4] Tagare DM. *Electricity Power Generation: The Changing Dimensions*. Hoboken, NJ: John Wiley & Sons; 2011.

[5] Ahmadi MH, Ghazvini M, Sadeghzadeh M, Alhuyi Nazari M, Kumar R, Naeimi A, et al. Solar power technology for electricity generation: A critical review. *Energy Science & Engineering*. 2018; 6(5): 340–361. Available from: https://doi.org/10.1002/ese3.239.

[6] Breeze P. *Power Generation Technologies*. Oxford: Newnes; 2019.

[7] Erenoğlu AK, Erdinç O, Taşcıkaraoğlu A. History of electricity. In: *Pathways to a Smarter Power System*. London: Academic Press; 2019. p.1–27.

[8] David PA, Bunn JA. The economics of gateway technologies and network evolution: Lessons from electricity supply history. *Information Economics and Policy*. 1988; 3(2): 165–202. Available from: https://doi.org/10.1016/0167-6245(88)90024-8.

[9] Du Boff RB. The introduction of electric power in American manufacturing. *The Economic History Review*. 1967; 20(3): 509–518. Available from: https://doi.org/10.2307/2593069.

[10] Breyer C, Khalili S, Bogdanov D, Ram M, Oyewo AS, Aghahosseini A. On the history and future of 100% renewable energy systems research. *IEEE Access*. 2022; 10: 78176–78218. Available from: https://doi.org/10.1109/ACCESS.2022.3193402.

[11] Madonna V, Giangrande P, Galea M. Electrical power generation in aircraft: Review, challenges, and opportunities. *IEEE Transactions on Transportation Electrification*. 2018; 4(3): 646–659. Available from: https://doi.org/10.1109/TTE.2018.2834142.

[12] Kumar Dora B, Bath S, Mitra A, Ernst D, Halinka A, Zychma D, et al. The global electricity grid: A comprehensive review. *Energies*. 2025; 18(5): 1152. Available from: https://doi.org/10.3390/en18051152.

[13] Pal DB, Rathoure AK. Environmental aspects in electrical energy generation: A comprehensive review. In: *Renewable Energy Development: Technology, Material and Sustainability*. Singapore: Springer; 2025. p.351–375.

[14] Wei Y, Khojasteh D, Windt C, Huang L. An interdisciplinary literature review of floating solar power plants. *Renewable and Sustainable Energy Reviews*. 2025; 209: 115094. Available from: https://doi.org/10.1016/j.rser.2024.115094.

[15] Khare V, Nema S, Baredar P. Solar-wind hybrid renewable energy system: A review. *Renewable and Sustainable Energy Reviews*. 2016; 58: 23–33. Available from: https://doi.org/10.1016/j.rser.2015.12.223.

[16] Babaremu K, Olumba N, Chris-Okoro I, Chuckwuma K, Jen TC, Oladijo O, et al. Overview of solar-wind hybrid products: prominent challenges and possible solutions. *Energies*. 2022; 15(16): 6014. Available from: https://doi.org/10.3390/en15166014.

[17] Gupta SC, Kumar Y, Agnihotri G. Optimal sizing of solar-wind hybrid system. In: *IET-UK International Conference on Information and Communication Technology in Electrical Sciences (ICTES 2007)*. Stevenage, UK: Institution of Engineering and Technology (IET); 2007. p.282–287.

[18] Badwawi RA, Abusara M, Mallick T. A review of hybrid solar PV and wind energy system. *Smart Science*. 2015; 3(3): 127–138. Available from: https://doi.org/10.1080/23080477.2015.11665647.

[19] Malik MZ, Zehra K, Ali I, Ismail M, Hussain A, Kumar V, et al. Solar-wind hybrid energy generation system. In: *2020 IEEE 23rd International Multitopic Conference (INMIC)*. Bahawalpur, Pakistan: IEEE; 2020. p.1–6.

[20] Ponnapalli B, Lakshmikhandan K, Palanisamy K, Sithambaram M. A hybrid technique for grid-connected solar-wind hybrid system with electric vehicles. *Energy & Environment*. 2024; 35(5): 2753–2789.

[21] Singh S, Singh M, Kaushik SC. A review on optimization techniques for sizing of solar-wind hybrid energy systems. *International Journal of Green Energy*. 2016; 13(15): 1564–1578. Available from: https://doi.org/10.1080/15435075.2016.1207079.

[22] Chen HH, Kang HY, Lee AH. Strategic selection of suitable projects for hybrid solar-wind power generation systems. *Renewable and Sustainable Energy Reviews*. 2010; 14(1): 413–421. Available from: https://doi.org/10.1016/j.rser.2009.08.004.

[23] Sabatier JA, Agrawal OP, Machado JT. *Advances in Fractional Calculus*. Dordrecht: Springer; 2007.

[24] Herrmann R. *Fractional Calculus: An Introduction for Physicists*. Singapore: World Scientific; 2011.

[25] Caputo M, Fabrizio M. A new definition of fractional derivative without singular kernel. *Progress in Fractional Differentiation & Applications*. 2015; 1(2): 73–85.

[26] Bas E, Acay B, Ozarslan R. Fractional models with singular and non-singular kernels for energy efficient buildings. *Chaos: An Interdisciplinary Journal of Nonlinear Science*. 2019; 29(2): 023110. Available from: https://doi.org/10.1063/1.5082390.

[27] Khan A, Abdeljawad T, Abdel-Aty M, Almutairi DK. Digital analysis of discrete fractional order cancer model by artificial intelligence. *Alexandria Engineering Journal*. 2025; 118: 115–124. Available from: https://doi.org/10.1016/j.aej.2025.01.036.

[28] Ali S, Khan A, Shah K, Alqudah MA, Abdeljawad T, Siraj-ul-Islam. On computational analysis of highly nonlinear model addressing real world applications. *Results in Physics*. 2022; 36: 105431. Available from: https://doi.org/10.1016/j.rinp.2022.105431.

[29] Ravichandran C, Logeswari K, Khan A, Abdeljawad T, Gómez-Aguilar JF. An epidemiological model for computer virus with Atangana-Baleanu fractional derivative. *Results in Physics*. 2023; 51: 106601. Available from: https://doi.org/10.1016/j.rinp.2023.106601.

[30] Atangana A. Fractal-fractional differentiation and integration: Connecting fractal calculus and fractional calculus to predict complex system. *Chaos, Solitons & Fractals*. 2017; 102: 396–406. Available from: https://doi.org/10.1016/j.chaos.2017.04.027.

[31] Atangana A, Qureshi S. Modeling attractors of chaotic dynamical systems with fractal-fractional operators. *Chaos, Solitons & Fractals*. 2019; 123: 320–337. Available from: https://doi.org/10.1016/j.chaos.2019.04.020.

[32] Atangana A, Araz Sİ. Atangana-Seda numerical scheme for labyrinth attractor with new differential and integral operators. *Fractals*. 2020; 28(8): 2040044. Available from: https://doi.org/10.1142/S0218348X20400447.

[33] Ma Z, Zahed H, Ahmad J. Fixed point results with applications to fractional differential equations of anomalous diffusion. *Fractal and Fractional*. 2024; 8(6): 318. Available from: https://doi.org/10.3390/fractalfract8060318.

[34] Chugunov V, Fomin S. Application of fractional differential equations for modeling bacteria migration in porous medium. *Mathematics*. 2024; 12(5): 685. Available from: https://doi.org/10.3390/math12050685.

[35] Matlob MA, Jamali Y. The concepts and applications of fractional order differential calculus in modeling of viscoelastic systems: A primer. *Critical Reviews in Biomedical Engineering*. 2019; 47(4): 249–276. Available from: https://doi.org/10.1615/CritRevBiomedEng.2018028368.

[36] Sheng H, Chen Y, Qiu T. *Fractional Processes and Fractional-Order Signal Processing: Techniques and Applications*. London, UK: Springer Science & Business Media; 2011.

[37] Katok A, Katok AB, Hasselblatt B. *Introduction to the Modern Theory of Dynamical Systems*. Cambridge, UK: Cambridge University Press; 1995.

[38] Kumar VR, Mani N. The application of artificial intelligence techniques for intelligent control of dynamical physical systems. *International Journal of Adaptive Control and Signal Processing*. 1994; 8(4): 379–392. Available from: https://doi.org/10.1002/acs.4480080407.

[39] Böttcher L, Antulov-Fantulin N, Asikis T. AI Pontryagin or how artificial neural networks learn to control dynamical systems. *Nature Communications*. 2022; 13(1): 333. Available from: https://doi.org/10.1038/s41467-021-27590-0.

[40] Yuksel G. Dynamical systems and artificial intelligence. In: *Artificial Intelligence*. Boca Raton, FL, USA: CRC Press; 2024. p.75–83.

[41] Sharma P, Khan JS, Radhika K, Thatipudi JG, Sridevi K, Upadhyay S. Evolutionary intelligence: A hybrid neural framework for dynamic system innovation. In: *2025 International Conference on Electronics and Renewable Systems (ICEARS)*. Tuticorin, India: IEEE; 2025. p.1743–1749.

[42] Khan H, Alfwzan WF, Alzabut J, Almutairi DK, Azim MA, Thinakaran R. Artificial intelligence and neural networking for an analysis of fractal-fractional Zika virus model. *Fractals*. 2025; 33(8): 2540143. Available from: https://doi.org/10.1142/S0218348X25401437.

[43] Khan H, Alzabut J, Almutairi DK, Alqurashi WK. The use of artificial intelligence in data analysis with error recognitions in liver transplantation in HIV-AIDS patients using modified ABC fractional order operators. *Fractal and Fractional*. 2025; 9(1): 16. Available from: https://doi.org/10.3390/fractalfract9010016.

[44] Khan H, Alzabut J, Tounsi M, Almutairi DK. AI-based data analysis of contaminant transportation with regression of oxygen and nutrients measurement. *Fractal and Fractional*. 2025; 9(2): 125. Available from: https://doi.org/10.3390/fractalfract9020125.

[45] Mohammad SI, Al-Momani AA, Vasudevan A, Masadeh M, Al Sarayreh A, Jahmani K, et al. Innovation through intelligence: Mapping the adoption of artificial intelligence with bibliometric methods. In: *Artificial Intelligence, Sustainable Technologies, and Business Innovation: Opportunities and Challenges of Digital Transformation*. Cham: Springer Nature Switzerland; 2025. p.187–198.

[46] Wan-Arfah N, Muzaimi M, Naing NN, Subramaniyan V, Wong LS, Selvaraj S. Prognostic factors of first-ever stroke patients in suburban Malaysia by comparing regression models. *Electronic Journal of General Medicine*. 2023; 20(6): em545. Available from: https://doi.org/10.29333/ejgm/13717.

[47] Devi A, Kumar A, Abdeljawad T, Khan A. Existence and stability analysis of solutions for fractional langevin equation with nonlocal integral and anti-periodic-type boundary conditions. *Fractals*. 2020; 28(8): 2040006. Available from: https://doi.org/10.1142/S0218348X2040006X.